Received: 25 May 2024 | Accepted: 7 August 2024

DOI: 10.1002/appl.202400097

RESEARCH ARTICLE

Applied Research

Impedance-based monitoring of titration and neutralization assays with VSV-G and SARS-CoV-2-spike pseudoviruses

Anne-Kathrin Mildner[1] | **Sebastian Einhauser**[2] | **Stefanie Michaelis**[3] | **Klara Rogalla v. Bieberstein**[1] | **Ralf Wagner**[2,4] | **Joachim Wegener**[1,3]

[1]Institut für Analytische Chemie, Chemo- und Biosensorik, Universitaet Regensburg, Regensburg, Germany

[2]Institut fuer Medizinische Mikrobiologie und Hygiene, Universitaet Regensburg, Regensburg, Germany

[3]Fraunhofer-Institut für Elektronische Mikrosysteme und Festkoerper-Technologien EMFT, Regensburg, Germany

[4]Institut fuer Klinische Mikrobiologie und Hygiene, Universitätsklinik Regensburg, Regensburg, Germany

Correspondence

Joachim Wegener, Institut für Analytische Chemie, Chemo- und Biosensorik, Universitaet Regensburg, Regensburg, Germany.
Email: Joachim.Wegener@ur.de

Funding information

Bundesministerium für Bildung und Forschung, Grant/Award Number: FKZ 13XP5085; Fraunhofer-Gesellschaft; Bayerisches Staatsministerium für Wissenschaft und Kunst

Abstract

Since cell-based virus neutralization assays are still the gold standard to assess a patient's immune protection against a given virus, they are of utmost importance for serodiagnosis, convalescent plasma therapy, and vaccine development. Monitoring the emergence and characteristics of neutralizing antibodies in an outbreak situation, confirming neutralizing antibodies as correlates of protection from infection and testing vaccine-induced potency of neutralizing antibody responses, quests for automated, fast, and parallel neutralization assays. We developed an impedance-based sensor platform (electric cell-substrate impedance sensing, ECIS) providing time-resolved monitoring of the host cell response to viral pseudotypes. For validation, the impedance assay was compared with state-of-the-art quantification of virus-induced reporter protein expression as an independent indicator of virus infection and neutralization. Vesicular stomatitis virus (VSV) derived pseudoviruses encoding the green fluorescent protein (GFP) as reporter and the autologous G protein (VSV-G) for the initial binding to the host cell membrane were used for monitoring of HEK293T cell infection and neutralization with both, impedance and optical readout. Virus-induced cytopathic effects (CPE) were detectable for low pseudotype concentrations (multiplicity of infection 1) in time-resolved impedance profiles as soon as 5–10 h after infection in a concentration-dependent manner. Neutralization efficacy of α-VSV-G antibodies was determined from impedance time courses and IC_{50} values compared favorably with fluorescence measurements of virus-borne GFP expression. Sera of convalescent COVID-19 patients were tested successfully for SARS-CoV-2 neutralizing antibodies by incubating VSV, pseudotyped with the SARS-CoV-2 spike protein, with different sera before host cell exposure and impedance recordings. In summary: (i) ECIS monitoring was successfully applied to detect virus-mediated cell infection and neutralization; (ii) Impedance-based monitoring allows reducing the assay time to 5–10 h; and (iii) the platform is easily adapted to other virus-based diseases and scalable to high-throughput.

KEYWORDS
ECIS, electric cell-substrate impedance sensing, label-free, neutralizing antibody, reporter gene assay, virus neutralization assay, virus titer

INTRODUCTION

Virus neutralization tests are routinely applied in various biomedical disciplines including virology, immunology, epidemiology, and vaccine development as they are the only assay to distinguish neutralizing from non-neutralizing (binding) antibodies. Testing the neutralization potential of antibodies in serological samples plays a fundamental role in evaluating the efficacy of the neutralizing immune response, which is particularly crucial in vaccine development [1]. In 2019, a novel RNA virus named severe acute respiratory syndrome coronavirus 2 (SARS-CoV-2) emerged and spread around the globe. The ensuing COVID-19 pandemic triggered a race against time for the development of efficient vaccines [2]. A remarkable number of serological assays had to be conducted to primarily monitor convalescent and vaccine-induced immunity against the virus [3].

The plaque reduction neutralization test still stands as the gold standard in neutralization assays, indicating the presence of neutralizing antibodies and predicting the level of protection of the blood donor against infection. These assays involve exposing virus-sensitive host cells to mixtures of the target virus and antibody-containing serum samples, followed by detection of potential cytopathic effects (CPEs) within the host cells over several days. Visual detection of plaques (i.e. regions of host cell destruction) indicates insufficient virus neutralization [4]. However, these assays are known for their substantial time requirements and high laboratory workload [5]. Additionally, working with replication competent SARS-CoV-2 viruses requires biosafety level (BSL)−3 and all the regimentations that come with it. To overcome the labor-intense nature and limited potential for automation, various assays for SARS-CoV-2 neutralization have been developed in recent years, including those employing virus surrogate neutralization assays (sNA) or pseudovirus neutralization assays (pNA) [3].

pNAs have gained popularity as a research tool, mimicking both the virus-receptor binding and cell entry mechanisms. Pseudoviruses retain the infectivity of the original virus but are replication-incompetent, allowing experimental work in lower BSL laboratories (BSL1-2) [4]. Typically, direct or inducible reporters are introduced into the genome of the pseudoviruses to facilitate the detection of infected cells by reporter protein expression. Established systems use reporter proteins such as the green fluorescent protein (GFP) or a luciferase [6–9].

In this study, pseudotypes of the vesicular stomatitis virus (VSV), engineered to present either the autologous glycoprotein (VSV-G) or the SARS-CoV-2 spike protein on the virus surface, were used to establish an impedance-based readout of viral cell infection. Moreover, both pseudotypes were engineered to carry a GFP gene for correlation of impedance results with the assessment of reporter gene expression in the host cells. The original VSV-G enters a wide range of host cells by binding to host cell receptors via the glycoprotein G and subsequent fusion with the cellular membrane. Following entry, viral replication is initiated by the release of the single-stranded, negative-sense RNA genome encoding viral proteins like nucleocapsid (N), phosphoprotein (P), matrix protein (M), glycoprotein (G), and large protein (L) followed by their expression using the host cells' protein synthesis machinery [10, 11]. As viral replication progresses and high numbers of viruses are produced, host cells show increasingly severe, virus-induced CPEs leading ultimately to cell death. It has been reported by others, that the M protein induces apoptosis in host cells [12] and is responsible for subsequent cell lysis [13, 14]. Replication incompetent VSV-based pseudotypes have been widely used to mimic other viruses by integrating their surface proteins into the VSV-genome. In our research, for instance, the VSV is pseudotyped with the wildtype SARS-CoV-2 spike protein (S2) lacking the ER retention signal to support efficient display on the VSV particle surface [15]. This enables cell entry, initialized through binding of the SARS-CoV-2 spike protein to its cognate receptor, the human angiotensin-converting enzyme 2 (ACE2). The latter is exposed on the surface of human embryonic kidney cells overexpressing ACE2. Recognition by the ACE2 receptor triggers various protease-mediated trimming steps and conformational changes of the SARS-CoV-2 spike protein, ultimately facilitating fusion between viral and cellular membranes and leading to infection of the target cell [4, 16] (Figure 1a).

Electric cell-substrate impedance sensing (ECIS) is a well-established and versatile method to monitor various phenotypes of adherent cells, like motility, proliferation, or the various forms of cell death. The technique is based on measuring the impedance of cells grown on small gold-film electrodes with low-amplitude AC signals [19]. When healthy cells attach and spread on the electrode, the electrode impedance increases as the dielectric cell bodies restrict current flow compared to the cell-free electrode. When the electrode is confluently covered, impedance measurements report on rather small changes in cell morphology below the limits of regular wide-field optical microscopy [20]. We recorded the impedance of appropriate host cells while being exposed to different concentrations of the VSV-G and VSV-SARS-CoV-2 pseudoviruses to follow the time course of infection. The experiments were repeated in presence of purified antibodies or serum mixtures to test for their neutralizing capacity. Impedance data were then compared to expression levels of virus-borne GFP. Both assays returned similar results. Lytic properties of VSV-based pseudoviruses facilitated an early detection of host cell infection by impedance measurements already after 5–10 h. Electric Cell-Substrate Impedance Sensing (ECIS) provides a highly automated, scalable, and label-free platform to conduct neutralization assays and virus titration in real time.

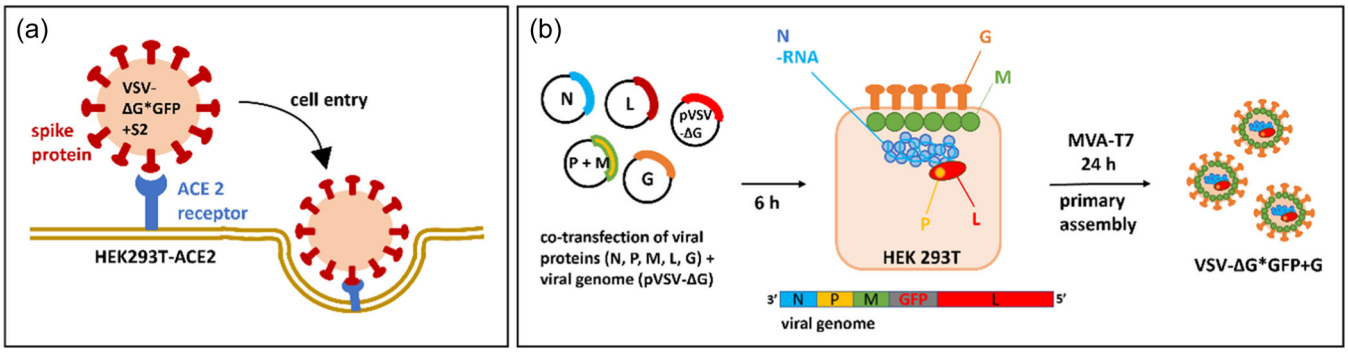

FIGURE 1 (a) Schematic illustrating cell entry of VSV-ΔG*GFP + S2. Membrane fusion and viral uptake are initiated by binding of the viral spike protein S2 to the human angiotensin-converting enzyme 2 (ACE2) receptor of host cells [4]. (b) Assembly of VSV-ΔG*GFP + G pseudoviruses in HEK293T cells. The viral nucleocapsid protein (N), glycoprotein (G), matrix protein (M), large polymerase subunit (L), and phosphoprotein (P) are expressed in transfected HEK cells. In the presence of a virus-borne T7 RNA polymerase (MVA-T7), the viral genome is expressed. Depletion of the envelope protein (G) and insertion of green fluorescent protein (GFP) in the viral genome led to replication incompetence and expression of GFP in host cells after infection [17, 18].

MATERIALS AND METHODS

Cell lines

Human embryonic kidney 293T (HEK293T) cells and HEK293T-ACE2 cells, stably transfected with the human angiotensin-converting enzyme II (hACE2) cells were grown in Dulbecco's modified Eagle's medium with 4.5 g/L D-glucose (DMEM; Sigma) supplemented with 10% (v/v) fetal bovine serum (FBS; Thermo Fisher Scientific), 100 µg/mL penicillin (Sigma) and 100 µg/mL streptomycin (Sigma). For HEK293T-ACE2 cells, 100 µg/mL hygromycin B (Invitrogen) was added to the culture medium to retain selection pressure. The cells were kindly provided by Dr. Janine Kimpel (Medical University of Innsbruck, Austria) [21]. Baby Hamster kidney (BHK-21-VSV-G) cells expressing the VSV glycoprotein G were kindly provided by Prof. Dr. Stefan Pöhlmann (DPZ Göttingen). These cells were grown in DMEM supplemented with 10% (v/v) fetal bovine serum (FBS; Thermo Fisher Scientific), 100 µg/mL penicillin (Sigma), 100 µg/mL streptomycin (Sigma), 1x non-essential amino acids (NEAA; Gibco) and 1 mM NaPyruvate (Gibco). BHK-21-VSV-G cells were selected with 100 µg/mL zeocin (Invivogen) and 50 µg/mL hygromycin (Invivogen) every fourth passage. Cell lines were maintained at 37°C in a humidified incubator with 5% CO_2 and passaged every 3–4 days.

Generation of VSV pseudoviruses

Two types of pseudoviruses derived from the vesicular stomatitis virus (VSV) were used. VSV-ΔG*GFP + G pseudoviruses, initially lacking the autologous VSV-G protein, were generated by insertion of the GFP coding sequence in pVSV-ΔG-N/P-MCS2-2.6 (Kerafast; #551 with Helper Plasmids-(A)) vector backbone using the multiple cloning site 2 (MCS-2). Viral particles were rescued using the protocol by Whitt [22]. For the recovery of VSV-G pseudotypes, 5×10^5 HEK293T cells were seeded into each well of a 6-well plate and transfected with 200 µL transfection mix containing 17 µg of the helper plasmids (VSV-N, VSV-P, VSV-G, VSV-L; Kerafast) encoding the viral proteins N, P, G, and L in a ratio of 3:5:8:1, 5 µg of pVSV-ΔG*GFP and 50 µg polyethylenimin (PEI; Polysciences; #26008) as chemical transfection reagent. After 6 h of incubation at 37°C, the transfection mix was removed and sonicated. MVA-T7 (modified vaccinia ankara virus carrying the RNA polymerase T7) was added to each well at MOI 5 (cf. Figure 1b). Virus recovery supernatants were harvested 24 h post-transfection and centrifuged at 2000*g* for 2 min. For amplification, BHK-21-VSV-G cells, induced to express the VSV glycoprotein G by 10^{-9} M mifepristone (Sigma Aldrich, #m8046), were infected with the filtered virus supernatants (0.22 µm Rotilabo-PVDF syringe filter, Roth). When 40%–100% of cells showed cytopathic effects and GFP expression, usually within 24–48 h, supernatants were harvested and centrifuged at 2000*g* for 2 min. The virus titer was quantified by the *limited dilution plaque forming assay*. Suspensions of the generated VSV-ΔG*GFP + G pseudovirus were stored at −80°C.

VSV pseudotyped with the SARS-CoV-2 spike protein (VSV-ΔG*GFP + S2) were generated in HEK293T cells as described previously [17, 23]. In brief, 5×10^5 HEK293T cells were seeded in each well of a six-well plate and transfected with 50 ng pEVAC-SARS-CoV-2 Spike-dER using (50 µg) PEI on the next day. 20 h post-transfection, cells were infected with VSV-ΔG*Luc-G (MOI 4) for 2 h. Then, medium was exchanged and excess VSV-ΔG*Luc-G was neutralized using the antibody α-VSV-G (8G5F11, mouse, absolute antibody; Kerafast). The next day, supernatants were collected, centrifuged for 10 min at 2000*g* and stored at −80°C. Pseudoviral titers were determined by limited dilution on HEK293T-ACE2 cells and fluorescence microscopy.

Antisera and monoclonal antibodies

The recombinant monoclonal antibody α-VSV-G (8G5F11; mouse, absolute antibody; Kerafast) was used for the neutralization of

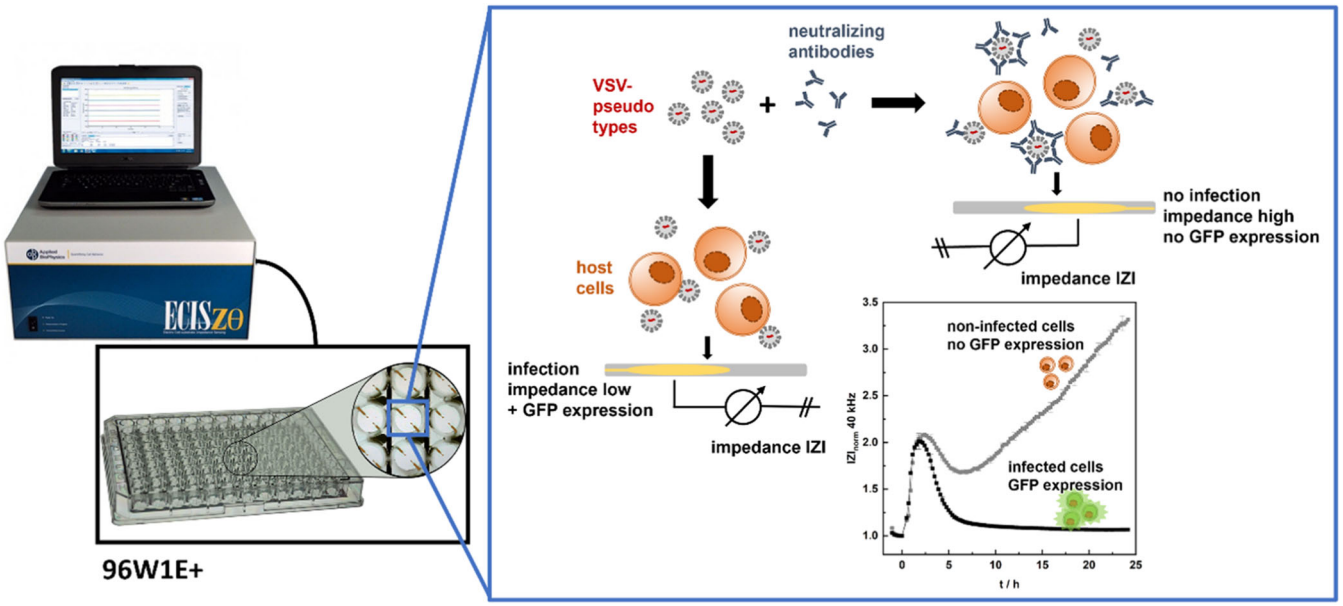

FIGURE 2 Schematic concept of impedimetric monitoring of vesicular stomatitis virus (VSV)-infection of host cells in presence or absence of neutralizing antibodies. The ECIS-ZΘ platform from Applied BioPhysics [26] was used in combination with 96W1E+ electrode arrays [26] (left). Suspensions of host cells were mixed with a well-defined suspension of VSV-pseudotypes and antibodies. The mixture was allowed to settle on gold-film electrodes. The electrode impedance at 40 kHz was recorded as a function of time and served as an indicator for cytopathic effects (right).

VSV-ΔG*GFP + G and stored in a 0.1 mg/mL stock solution in PBS^{++} at 4°C. Sera from the TiKoCo19 cohort were tested for neutralization of VSV-ΔG*GFP + S2 (approved by the Ethics Committee of the University of Regensburg, Germany (vote 20-1867-10) [24]. The sera were heat-inactivated for 30 min at 60°C and stored at −80°C. *Serum 1* is a pooled mix of neutralizing sera containing antibodies against SARS-CoV-2 derived from 50 patients after infection/vaccination. *Serum 2* is from an individual after COVID-19 infection, whereas *serum 3* is a non-neutralizing serum collected from people who neither had a SARS-CoV2 infection nor have they been vaccinated. *Serum 3* serves as a control.

Limited dilution plaque-forming assay

10^5 HEK293T cells were seeded in a volume of 100 µL medium in each well of a 96-well plate before they were exposed to 100 µL of VSV-ΔG*GFP + G pseudovirus dilutions from 1:10 to $1:10^8$ in steps of one order of magnitude. Cells and viruses were incubated at 37°C and 5% CO_2 for 24 h to ensure stable protein expression. GFP-positive cells were counted and defined as a plaque-forming unit. Based on this, titers of pseudovirus stock solutions were diluted to the required multiplicity of infection (MOI) with DMEM before the experiment.

Impedance-based monitoring of host cell infection

Electric cell-substrate impedance sensing (ECIS) uses the electrochemical impedance of thin-film electrodes to monitor phenotypic assays with adherent cells noninvasively, label-free, and with high time resolution that is easily reduced to a few seconds [25]. The ECIS principle relies on a two-electrode configuration, realized by depositing two planar gold-film electrodes (50 nm) on the bottom of cell-culture plates (cf. Figure 2). The electrical connection between the electrodes is provided through the conducting nature of physiological buffers like cell culture medium. When cells attach and spread on the electrode surface, they act as small insulating particles. Their membranes constrict the current, forcing it to flow beneath the cells and through narrow clefts between neighboring cells for frequencies below 10 kHz. At frequencies higher than 10 kHz the current capacitively couples through the cell membranes. The frequency-dependent impedance IZI reports very sensitively on changes in cell shape and electrode coverage dependent on the AC frequency [27]. This study was conducted using the ECIS-ZΘ platform manufactured by Applied BioPhysics Inc. in combination with their proprietary 96W1E+ electrode arrays to monitor HEK293T and HEK293T-ACE2 cells during infection with VSV-derived pseudotypes and subsequent cytopathic effects. Briefly, the 96W1E+ electrode arrays were exposed to argon plasma for 30 s to clean the gold surface from atmospheric adsorbents. Electrodes in each well were coated with cross-linked gelatin by incubation with 0.5% (w/v) gelatin in H_2O for 1.5–2 h followed by cross-linking with 2.5% glutaraldehyde in water for 10 min and flooding the wells 8–10 times with water. Baseline impedance at 40 kHz was recorded for 1-2 h using 100 µL cell culture medium per well. Suspensions of HEK cells were adjusted to a cell density of 10^6 cells/mL before the assay. One hundred microliters of this cell suspension was added to each well and mixed with VSV-ΔG*GFP pseudoviruses at MOI 0-10, respectively. The

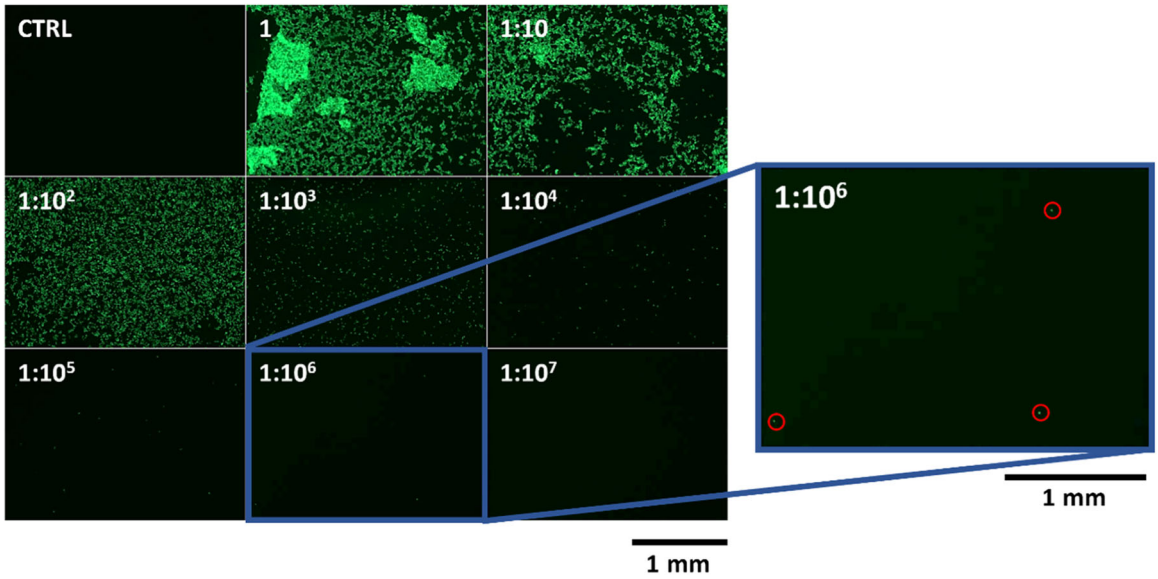

FIGURE 3 Fluorescence micrographs of virus-induced green fluorescent protein (GFP) expression in HEK293T cells after treatment with different dilutions of VSV-ΔG*GFP + G. Red circles indicate GFP-positive cells after vesicular stomatitis virus (VSV) infection (zoom in, right). Virus titer was calculated from the GFP-positive cell counts when a dilution of $1:10^6$ was applied.

impedance was then recorded for 24 h reporting on the individual virus–cell interactions in each well.

Impedance-based monitoring of pseudovirus neutralization

Preparation of electrode array and cell suspension was conducted as described in the preceding section. For neutralization, VSV-ΔG*GFP + G pseudoviruses were diluted with DMEM to a concentration of MOI 1 (1×10^6 ffu/mL) and mixed with the α-VSV-G antibody in final concentrations from 0 to 10 µg/mL. The immune complexes were incubated at 37°C for 1 h before 10^5 HEK293T suspended in 100 µL medium were added to the antibody–virus mixture in each well. Impedance was then monitored for 24 h. For neutralization of VSV-ΔG*GFP + S2 with sera 1–3, suspensions of 1.8×10^7 ffu/mL pseudoviruses (corresponding to MOI 15) were prepared in culture medium. Mixtures of 20 µL blood serum and 80 µL of the virus suspension were mixed and incubated for 1 h at 37°C. After this incubation, 10^5 HEK293T-ACE2 cells were added to each well, and impedance was recorded for 24 h.

Impedance data analysis

The time-dependent impedance magnitude $|Z|$, recorded at an AC frequency of 40 kHz, was normalized by division to the individual impedance magnitude $|Z|$ of the cell-free electrodes before the cell-virus mixtures were added to the wells. The resulting time courses of the normalized impedance $|Z|_{norm}$ were integrated (area under the curve, AUC) between 0 and 24 h using $|Z|_{norm} = 1$ as a constant baseline. Effective and inhibitor concentrations with 50% efficiency (TCID50, IC_{50}) were calculated via a four-parameter logistic fit using the data analysis software Origin 2022. Spearman and Pearson correlation coefficients were calculated using Matlab R2024a.

Determination of infectivity via fluorescence intensity

After 24 h of impedance recording, integral fluorescence intensity was determined for every well of the ECIS electrode array using a TECAN GENios (top read, $\lambda_{exc} = 485$ nm, $\lambda_{em} = 535$ nm, gain: 73). Spatial mapping of fluorescence in selected wells of the electrode arrays was accomplished by fluorescence microscopy (Nikon eclipse Ts2FI inverse microscope ($\lambda_{exc} = 470$ nm (LED); $\lambda_{em} = 510$ nm). Pictures were taken with 4× magnification and 400 ms exposure time.

RESULTS

Determination of virus titer via limited dilution focus-forming assay

VSV-ΔG*GFP + G pseudoviruses displaying the autologous VSV-G protein on the virus particle surface successfully infected HEK293T cells for virus dilution of $1:10^7$ or lower as determined from green fluorescent protein emission (reporter gene product). Cells expressing virus-borne GFP fluorescence were counted after infection with a VSV-ΔG*GFP + G suspension at a dilution of $1:10^6$. Considering this dilution factor, the virus titer was determined to be 8.9×10^7 per mL. Decreasing infection of the target cells with increasing dilution factor of the pseudoviral stocks is demonstrated in Figure 3 by means of

typical fluorescence micrographs. We used the virus titer as determined from these experiments in all studies addressing VSV-ΔG*GFP + G titration or neutralization.

Impedance-based cell monitoring reports on target cell infection in real time

VSV-ΔG*GFP + G pseudotypes were added to suspended HEK293T cells and the response of the target cells was monitored for VSV-ΔG*GFP + G concentrations between MOI 0.005 and MOI 10. As shown in Figure 4a, an initial impedance increase was detected for the first 2.5 h to normalized impedances between 2.0 and 2.3 after the virus-cell mixtures were inoculated into the wells of the 96-well electrode array. The initial impedance increase (0–2.5 h) is due to the settling of the suspended cells upon the electrode surface followed by adhesion and the onset of cell spreading. This first increase was followed by an impedance decrease within the next 5 h that was transient for control conditions and lower virus loads but monotonic for higher virus concentrations. When virus concentrations were higher than MOI 2 (orange curve), impedance decreased almost to the normalized impedance of cell-free electrodes (black curve). However, fluorescence micrographs indicate that the cell layers are confluent at the end of the measurement even for the highest virus concentration of MOI 10. Accordingly, the loss of impedance during virus encounter is not due to cell detachment but cell shrinkage—which might be a morphological indicator for the onset of apoptosis.

The transient minimum of the impedance at 7.5 h for the control and those electrodes that received a rather low virus load is interpreted as morphological rearrangements of the cells and their cell-matrix junctions, which were found to be highly characteristic for HEK293T cells grown on cross-linked gelatin. The persistent increase of impedance observed after 7.5 h indicates the continuation of cell spreading, morphological rearrangement and the onset of proliferation, which are severely affected by increasing virus density. Virus-mediated cell lysis starts for virus concentrations as low as MOI 0.1. The system saturated for MOI greater than 5. For cells exposed to VSV-ΔG*GFP + G at MOI 0.01 and MOI 0.005, the impedance time

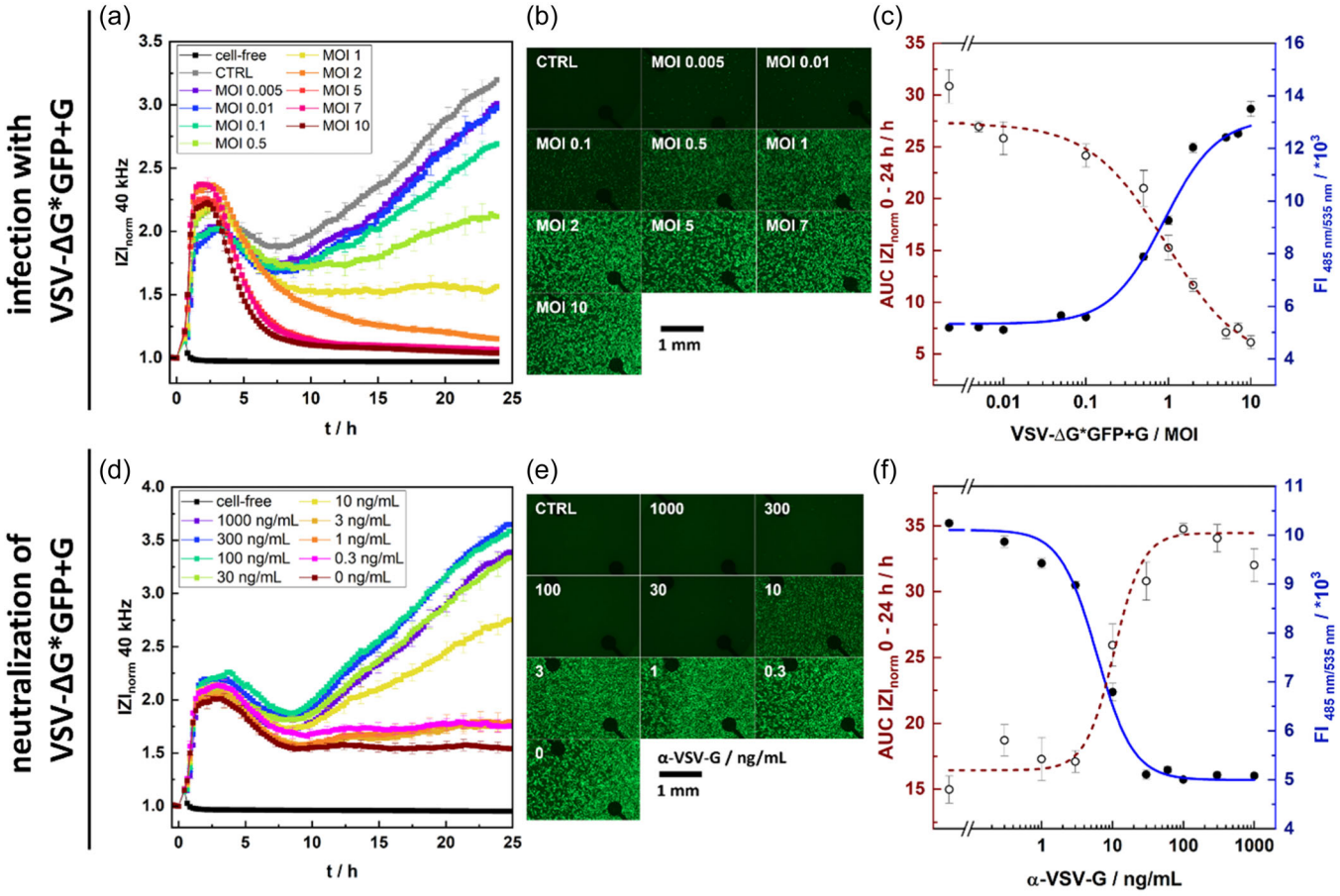

FIGURE 4 Time courses of impedance during host cell attachment in presence of VSV-ΔG*GFP + G (a) and neutralization with α-VSV-G antibodies (d). Fluorescence micrographs of virus-mediated green fluorescent protein (GFP) expression are used as an independent, orthogonal readout (b, e). $TCID_{50}$ values were calculated to be multiplicity of infection (MOI) 0.9 ± 0.2 from integrated impedance time courses and fluorescence intensities (FI), respectively (c). IC_{50} values of (11 ± 3) ng/mL (impedance) and (6.1 ± 0.9) ng/mL (FI) were determined from integrated impedance time courses or GFP fluorescence, respectively (f). All data are presented as mean ± SEM and $n = 8$. Data fitting was conducted using the data analysis software Origin (2022b) and a four-parameter logistic fit.

course followed the noninfected control (gray curve) indicating no significant influence of virus exposure. Interpretation of ECIS data regarding target cell infection was supported by integral fluorescence readings from every well and fluorescence microscopy of selected wells. Both fluorescence readouts document virus-mediated GFP expression in infected cells dependent on the virus load (Figure 4b). Fluorescence intensity increased significantly when host cells were exposed to higher virus titers. For the highest virus concentrations in this study (MOI 2–10) 100% of the target cell population showed GFP fluorescence after 24 h. Half of the cells were infected for virus concentrations around MOI 1, whereas MOI 0.005 and MOI 0.01 provided only individual cells with green fluorescence. The dark structures in the fluorescence micrographs correspond to the gold-film electrodes on the bottom of the well. $TCID_{50}$ values, calculated from integrated impedance time courses (0–24 h) or integral GFP fluorescence 24 h after virus exposure, respectively, were calculated to MOI (0.9 ± 0.2) and were identical for both readouts (Figure 4c). Support for this conclusion is provided by Spearman correlation analysis, which assesses how well the relationship between two variables is described by a monotonic function independent of their normal distribution. Perfect correlation provides a Spearman correlation coefficient of 1. For the correlation between impedance and fluorescence readouts of the titration experiments, calculation returned a Spearman coefficient of 0.873 ($p < 0.001$). The more often used Pearson correlation coefficient is used to describe a potential linear correlation. The calculation returned 0.861 ($p < 0.001$). Accordingly, monitoring the host cells by fully automated impedance readings or using the well-established reporter protein quantification provides highly correlated results and the same $TCID_{50}$ within error limits. It is noteworthy, that the impedance-based dose–response analysis is—different from the fluorescence readouts—available for any exposure time from one single experiment without any disturbance of the culture conditions.

Impedance-based neutralization assays with α-VSV-G antibodies

Neutralizing capabilities of antibodies against the VSV-surface protein (*α*-VSV-***G***) of VSV-ΔG*GFP + G were monitored by time-resolved ECIS measurements and, for benchmarking of the impedance data, by GFP fluorescence quantification. For this purpose, virus suspensions were adjusted to MOI 1 and pre-incubated with the VSV-G specific monoclonal antibody at concentrations ranging from 0.3 ng/mL to 1 µg/mL for 1 h in the wells of the electrode array before adding suspended HEK293T cells to these mixtures. Figure 4d shows the corresponding impedance time courses over 24 h after cell inoculation. In the first 7.5 h normalized impedance increased rather uniformly for all conditions to around 2.25 before all curves showed a decrease to a normalized value of around 1.75. In these first 5 h of the assay, the curves were not significantly different. Starting at $t = 10$ h, impedance time courses for antibody concentrations below 10 ng/mL followed the virus-only control (dark-red curve) showing a rather time-independent normalized impedance of 1.5 to 1.7. Differently, incubation with 10 ng/mL of α-VSV-G led to a partial neutralization of the pseudovirus impact on the target cells resulting in a slow but constant increase of the impedance over time. A strong impedance increase to values around 3.5 was observed when VSV-ΔG*GFP was neutralized with 0.1–1 µg/mL before target cell exposure. Findings from these impedance-based assays were verified by assessment of the reporter gene expression upon viral infection in presence of increasing concentrations of the neutralizing antibody (Figure 4e). Fluorescence micrographs show GFP fluorescence caused by VSV-ΔG*GFP infection only for antibody concentrations below 30 ng/mL. Looking at the number of GFP-positive cells after neutralization with 10 ng/mL α-VSV-G, half of the cells show green fluorescence and half of the population inside the well remained noninfected. $IC_{50,Z}$ values (Figure 4f) of (11 ± 3) ng/mL α-VSV-G, calculated from integrated impedance time courses (AUC), were found to be in line with conventional, state-of-the-art optical reporter gene readouts of virus-mediated GFP production in infected cells which was quantified to $IC_{50,\ GFP}$ = (6.1 ± 0.9) ng/mL α-VSV-G. Performing a correlation analysis of impedance and fluorescence readouts for the neutralization experiments returned a Spearman coefficient of 0.917 ($p < 0.005$) and a Pearson coefficient of 0.978 ($p < 0.001$) indicating a very strong, linear correlation between both readouts which supports the concept of using impedance measurements as tool to monitor neutralization assays. However, it remains to be tested whether the correlation is equally strong when other pseudotypes and/or other host cells are used in the experiments.

Impedance-based assays correctly report on the neutralizing capacity of patient sera towards SARS-CoV-2 pseudotypes

HEK293T-ACE2 cells genetically engineered to express the ACE2 receptor served as adherently growing target cells to test for the neutralizing capacity of patient sera with respect to SARS-CoV-2 pseudotypes. Within the first 2 h of the experiment, cell attachment to the electrode induced a transient impedance increase soon after seeding suspended target cells alone (gray, CTRL) or mixed with the VSV-ΔG*GFP + S2 pseudoviruses at MOI 15 (red, Figure 5a), respectively. Whereas the virus-free controls show a steady increase of impedance after 5 h, the impedance of the virus-loaded cells declines monotonically. After 24 h the impedance of virus-free host cells is app. 80% above the impedance of the cell-free electrode. At the same time, the impedance of virus-infected cells is just 20% above cell-free impedance indicating that infection with SARS-CoV-2 pseudotypes is readily detectable with this VSV-based model system. The rather high MOI used in these experiments became experimentally necessary as the target cells did not show a sufficiently robust impedance response for lower virus loads. However, significantly different time-dependent impedance profiles of infected and non-infected cells are a prerequisite to perform neutralization assays. In general, the impedance profiles of HEK293T-ACE2 cells differed

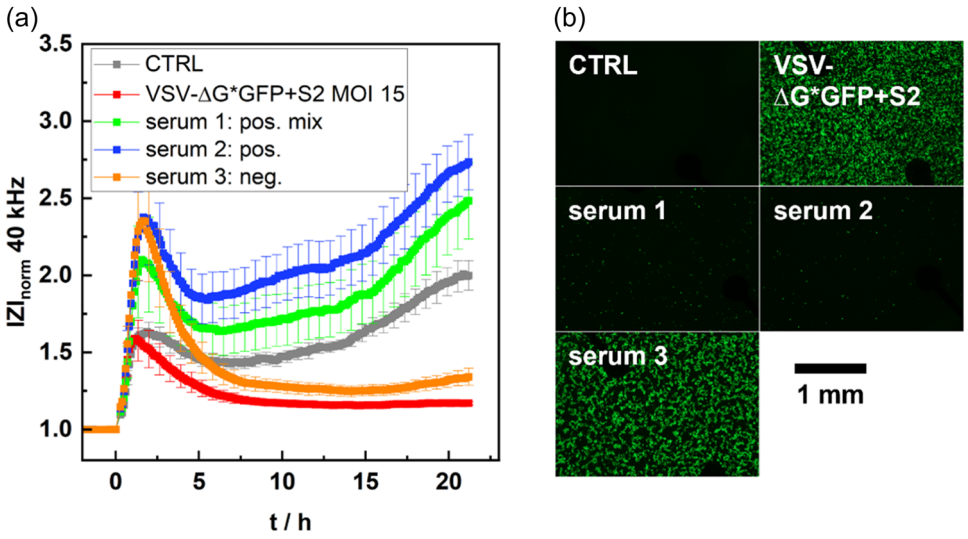

FIGURE 5 Time course of impedance to mirror host cell attachment in the absence (CTRL) or presence of SARS-CoV-2 pseudotypes and different human serum mixtures (a). Data are presented as mean ± SEM and $n = 3$. The respective fluorescence micrographs serve as optical controls for GFP reporter gene expression in case of virus infection (b).

from those shown in Figure 4a for the parental H293T cells in absence of any pseudotypes. We can only speculate about the underlying reasons. HEK293T-ACE2 went through genetic engineering and clonal selection. These rather invasive procedures may have returned a cell line that phenotypically differs from the parental cell line in more than just ACE2 expression. Since cell adhesion and spreading critically depend on the corresponding cell surface receptors (mostly integrins) and the mechanical properties of the plasma membrane, overexpression of ACE2—another cell surface receptor—may lead to interferences.

When patient sera (1,2,3) were added to the sample under test using the same number of target cells and pseudovirus particles, we observed that the initial impedance increase soon after cell seeding was significantly more pronounced. Since this response is independent of the neutralizing or non-neutralizing capacity of the sera (see below), it is straightforward to assume an unspecific impact of serum components on cell adhesion kinetics. Serum 1 (green) was pooled from the blood of 50 donors after infection or vaccination, whereas serum 2 (blue) was collected from a single patient after COVID-19 infection. Both sera show neutralizing capacity in the impedance-based neutralization assay, as the corresponding impedance time course show essentially the same profile as the virus-free control. This is most obvious as the impedance increases after 5 h of incubation rather than decreases. In contrast, serum 3 (orange) derived from a patient that was neither infected nor vaccinated, showed a similar impedance time profile as the one recorded for cells that were exposed to the pseudotypes only. Focusing on these experiments involving patient sera it is obvious that their neutralizing capacity becomes apparent as soon as 2 h after starting the experiment from the different slopes of the impedance decrease after passing the transient impedance maximum. Such an early assignment of neutralizing capacity is only accessible from time-resolved readouts with sufficiently high time resolution, as demonstrated for impedance measurements here.

Microscopic inspection after 24 h confirmed viral GFP reporter gene expression only in those cells that were infected by the pseudovirus in absence of neutralizing antibodies (Figure 5b). Whereas the virus-free control and co-incubation with serum 1/2 induced no significant fluorescence emission in the entire field of view. Unprotected exposure of the target cells to VSV-ΔG*GFP + S2 pseudotypes either alone or in presence of non-neutralizing serum 3 rendered most host cells GFP-positive.

DISCUSSION

In the previous section, we demonstrated on the example of two virus pseudotypes and their corresponding target cells that impedance measurements provide a time-resolved and highly automated alternative to conventional readouts for virus titration and neutralization assays. The experiments presented in this manuscript highlight some aspects of impedance-based readouts that will be discussed individually below. The different aspects rely mostly on the experiments with the VSV-ΔG*GFP + G pseudotype.

Impedance-based analysis of cell adhesion reports on virus load and presence of neutralizing antibodies

Titration experiments with VSV-ΔG*GFP + G revealed a clear dependence of the measured impedance on the actual virus load. Noninfected cells showed a continuous increase in impedance after attachment and spreading on the electrodes, visible 5 h after cell seeding. Infection of cells with VSV-ΔG*GFP + G at MOI 2 or higher,

however, led to an impedance decrease over time to values just slightly above the impedance of a cell-free electrode. These differences in the impedance time courses are most likely induced by cytopathic activity of the pseudoviruses ultimately inducing apoptosis and subsequent cell lysis [28]. It is well established that ECIS is capable of detecting apoptosis in adherent cells more sensitively than many biochemical assays that read caspase activity or DNA fragmentation [29]. As expected, the impact of virus infection does not affect the target cells immediately. The onset of measurable CPE requires several hours of exposure. Virus binding, uptake, and viral gene expression need time since the target cells are initially suspended in this assay and not adherently growing. Consistently, lowering the virus concentration from 2 to 0.1 viruses per cell (MOI) led to a reduced impact of the virus load on cell physiology in a concentration-dependent manner. At MOI 0.01 and 0.005 the target cell reaction was not distinguishable from the virus-free control; hence, cells remained healthy according to impedance measurements.

In virus neutralization assays, concentrations of the α-VSV-G antibody above 10 ng/mL neutralized VSV-ΔG*GFP + G at MOI 1 and resulted in impedance time courses following the typical adhesion characteristics of HEK293T cells with sequential phases of attachment, spreading, and proliferation of noninfected cells. When viruses were incubated with concentrations of 3 ng/mL and lower, neutralization of VSV-ΔG*GFP + G was not sufficient and host cells got infected as indicated by impedance values similar to cells exposed to a virus-only control (MOI 1). Analysis of the impedance time profiles returned a clear dose–response relationship. Reading the fluorescence of the GFP reporter provided highly similar results. Incubation of VSV-ΔG*GFP + G with α-VSV-G concentrations of 10 ng/mL neutralized the virus infection partially; higher concentrations completely protected the target cells from infection. For antibody concentrations lower than 10 ng/mL cells showed green fluorescence like the virus-only condition. Fluorescence readouts were performed immediately after the impedance measurement was terminated using the same cells in the same electrode array providing a perfect match for the correlation between impedance- and fluorescence-based readouts.

Benchmarking with established reporter gene assays

Findings from ECIS measurement were compared to the well-established method of virus-borne reporter gene expression. Here, GFP was used as an easy-to-detect reporter protein. In titration experiments, fluorescent micrographs showed GFP-positive cells for concentrations above MOI 0.1 similar to observations on viral impact from impedance measurements. To express infectivity of a given virus load in one number, impedance time courses were integrated along the whole measurement period of 24 h while fluorescence intensity was only recorded at a single time point (24 h). AUC and fluorescence intensity readings were fitted with a four-parameter logistic function providing $TCID_{50}$ for virus titration and IC_{50} for neutralization assays. The half-maximal tissue culture infectious dose $TCID_{50}$ of VSV-ΔG*GFP + G was determined to be MOI (0.9 ± 0.2), independent of the assay readout validating impedance-based analysis. In neutralization assays, IC_{50} values determined for α-VSV-G at MOI 1 were insignificantly different in impedance-based assays $IC_{50,Z}$ = (11 ± 3) ng/mL compared to the fluorescence intensity readout $IC_{50,\ GFP}$ = (6.1 ± 0.9) ng/mL. Correlation analysis (Spearman) demonstrated a strong correlation between the two independent observables impedance and fluorescence in both types of assays. Moreover, the results compare favorably with the literature. Munis et al. reported a half-maximal inhibitory concentration for α-VSV-G at MOI 0.8 of 11.5 ng/mL in 2018 [30].

The correlation between both readouts persisted also for the SARS-CoV-2 pseudotypes when the neutralizing capacity of patient sera was tested with respect to neutralizing antibodies against SARS-CoV-2. Sera were incubated with VSV-derived SARS-CoV-2 pseudotypes. Impedance decreased only for host cells exposed to viruses alone or when the virus samples were pre-incubated with the non-neutralizing serum 3 before host cell exposure. The constant increase of impedance, indicative of healthy cells, was only obtained for cells incubated with virus-free medium or exposed to viruses in presence of antibody-containing sera (serum 1 and 2). This pattern of cell infection was confirmed by fluorescence micrographs at the end of the impedance assays as an independent, orthogonal optical analysis of virus-borne GFP reporter gene expression in infected cells. Both readouts were found to be inline.

Comparing the impedance-readout with reporter gene assays in more detail, an important difference is noteworthy. Reporter gene assays are very specific. Expression of the reporter protein is exclusively limited to a host cell after successful infection with the virus that carries the reporter gene. Thus, the assay is not prone to false-positive readings. On the other hand, if virus infection or any other component of a sample under test interferes with protein biosynthesis in general or if reporter gene expression is retarded relative to other viral genes, the assay may read false-negative. The situation is inverted for impedance-based assays that are holistic in nature and operate without any inherent specificity. Since impedance reports also on functional impacts on cell physiology that are not caused by the viruses (e.g., change in osmolarity, presence of surface-active compounds, endogenous molecules that trigger signal transduction), it may report false positive, if the assay is not properly conducted and supported by stringent controls. But it will not fail to report on cytopathic effects for lytic viruses or pseudoviruses. Thus, it is very unlikely to provide false-negative answers.

Scalability and throughput

Impedance-based assays were performed in 96well plates with electrodes integrated in each well. Since impedance platforms are commercially available that allow for parallel tracking of six 96well electrode arrays in one assay or use 384well electrode arrays, impedance-based monitoring of titration and neutralization is clearly scalable to high throughput screening (HTS) formats. The suitability of a new assay for

HTS is often judged from its Z' value, which serves as a measure for the robustness of the assay. Z' is calculated from Equation (1):

$$Z' = 1 - \frac{3 \times (\sigma_p + \sigma_n)}{|\mu_p - \mu_n|}. \quad (1)$$

Herein, μ_p and μ_n denote the average of the positive (p) and negative (n) control, respectively, while σ_p and σ_n stand for their standard deviations. Z' of an ideal assay is 1.0. Assays performing better than 0.5 are considered useful for HTS [31]. When we use the upper asymptotes of the dose–response relationships in Figure 4 as values for the positive control and the lower asymptotes for the corresponding negative controls, the calculation returns Z' values of 0.64 for the titration assay and 0.70 for the neutralization assay based on impedance readings. These values indicate the robustness of both assays and their suitability for higher throughput campaigns. However, as will be further discussed below, this is very likely dependent on the nature of the virus or virus pseudotypes and their target cells. For comparison, we also calculated the Z' values for reporter gene-based titration and neutralization correspondingly. Z' values were found to be in the same range: 0.74 for titration and 0.88 for neutralization. Thus, both assay types are similarly *robust* and well above the threshold value of 0.5.

Assay time and time resolution

Results with replication-deficient VSV-ΔG*GFP + G pseudotypes showed that the time course of impedance during attachment and spreading of initially suspended HEK293T cells reports sensitively on the infection within 5–7 h. VSV is known to enter mammalian cells efficiently and quickly by binding of the envelope protein G to the low-density lipoprotein receptor on the cell surface initiating membrane fusion [32]. For comparison, conventional reporter gene assays typically require 20–24 h [33]. To demonstrate the potential of impedance-based analysis to provide shorter assay times, we have revisited the data regarding VSV-ΔG*GFP + G infection presented in Figure 4a. Instead of integrating from 0 h to 24 h to extract a measure for infectivity, we used the absolute values of the normalized impedance at $t = 10$ h for the different virus concentrations and determined the corresponding $TCID_{50}$ value (cf. Supporting Information: Figure S1). A $TCID_{50}$ value of MOI (1.6 ± 0.7) was obtained that is not significantly different from $TCID_{50}$ values determined from the integration of impedance profiles over 24 h or reading reporter gene expression after 24 h. Both approaches provided a $TCID_{50}$ of MOI (0.9 ± 0.2) after 24 h. This comparison underlines that time-resolved impedance readings provide the potential for significantly shorter assay times, saving 60% of experimental time in the example above. The reasons for the shorter response time of impedance measurements compared to reporter gene detection are not yet fully understood. Several factors may contribute. One of the critical details speeding up impedance-based assays as performed here is pseudovirus exposure of initially suspended target cells rather than pre-established adherent monolayers of target cells. We have studied the impact of virus encounter on established monolayers of host cells as well (data not shown). In these assays, the target cells were first grown to confluence before the virus suspension was added to the established cell layers. However, impedance readings reported less sensitive on the infection process even though we calculated—based on a physical model describing the impedance of cell-covered electrodes quantitatively [34]—that it takes less than 2 from 100 cells in a confluent HEK cell monolayer to be lysed for a significant and measurable impedance change (cf. Supporting Information: Figures S2 and S3). Experimentally, we have made similar observations regarding the difference between suspended and adherent 'sensor' cells with other stressors, like xenobiotic compounds or nanomaterials and conclude that suspended animal cells without a mature cytoskeleton—most notably the cortical actin—are more vulnerable than cells residing adherently on the surface. The concerted action of proteins involved in cell adhesion, spreading and morphological polarization is presumably very sensitive to any kind of cell stress or changes in cell physiology in this particular phase of anchorage-dependent cells leading to retardation of and interference with this process. Since virus impact on the host cells' adhesion machinery may be more direct and independent of protein biosynthesis, impedance readings indicate cell infections within less than 5–7 h after virus encounter. From a cellular perspective, this may serve as an explanation why impedance-based assays report sooner on host cell infection than reporter gene assays that depend on protein biosynthesis. Reporter gene readouts are typically carried out 20–24 h after virus addition ensuring stable expression of the reporter protein [33]. Since impedance data is recorded in real time and measurements are not invasive, dedicated data acquisition software tailored to this application could easily provide dose–response analysis 'on the fly' while virus exposure progresses in time. This may reduce the required assay time to a minimum and avoid any follow up data processing.

In summary, the experiments presented in this study clearly demonstrate that impedance readings may be used as label-free and time-resolved analysis in virus infection and neutralization assays providing many inherent technical advantages.

CONCLUSION

In this study, we have reported a platform technology based on electrochemical impedance measurements to monitor the host cell response upon viral infection in real-time. Even though it has been reported before that impedance measurements are a useful surrogate for more classical readouts [35], a stringent validation against established assays has not been presented yet. The direct comparison of impedance analysis and reporter gene assays for identical cell populations—as reported here—has closed this gap and paves the way for a more widespread use of label-free impedance analysis with all its technical benefits for virological assays like, for instance, virus titration or neutralization assays. The system is applicable to other viruses or virus-based diseases by changing the envelope protein of

the VSV pseudovirus and identifying the complementary host cells. It is noteworthy, that ECIS can only detect cytopathic changes in *adherent* but not *suspended* cells like blood cells. Ongoing research focuses on the development of experimental strategies to enhance the impact of non-lytic viruses on the impedance of their target cells since the former may otherwise not induce a significant impedance response of the latter. Without such amplifying mechanisms, the technique will be limited to cells that respond to virus encounter by changes in cell morphology or cell adhesion kinetics.

Due to the rather high time resolution of impedance measurements down to a few seconds, future assay developments will identify options for further reduced assay times compared to the canonical endpoint assays. This is particularly interesting since the time-dependent impedance profiles provide a fingerprint of the infection process with characteristic hallmarks that are most likely individual to the system under study. Finally, impedance-based monitoring of viral assays provides an unprecedented level of automation and throughput as commercial systems offer the capacity to monitor 6×96 samples simultaneously. The measurement is completely software-controlled and as such it provides the potential for automated data analysis routines that do not require any significant user input.

ACKNOWLEDGMENTS

The authors acknowledge financial support by the Fraunhofer-Anti-Corona-Program within the initiatives CoviRep and DRECOR and by the Bavarian Ministery of Science and Arts (Bay STMWK, FOR-COVID, F.2-F2412.32/1/45). Moreover, the authors acknowledge financial support by the Federal Ministry of Education and Research (BMBF) for the project ViroSens (project number FKZ 13XP5085) within the framework KMUinnovative. Technical support by David Brenner (Institut fuer Medizinische Mikrobiologie und Hygiene, Universitaet Regensburg) is also gratefully acknowledged. Open Access funding enabled and organized by Projekt DEAL.

CONFLICT OF INTEREST STATEMENT

The authors declare no conflict of interest.

DATA AVAILABILITY STATEMENT

The data that support the findings of this study are available from the corresponding author upon reasonable request.

ORCID

Joachim Wegener http://orcid.org/0000-0001-8554-0150

REFERENCES

[1] A. E. Muruato, C. R. Fontes-Garfias, P. Ren, M. A. Garcia-Blanco, V. D. Menachery, X. Xie, P.-Y. Shi, *Nat. Commun.* **2020**, *11*, 4059.
[2] K. R. Bewley, N. S. Coombes, L. Gagnon, L. McInroy, N. Baker, I. Shaik, J. R. St-Jean, N. St-Amant, K. R. Buttigieg, H. E. Humphries, K. J. Godwin, E. Brunt, L. Allen, S. Leung, P. J. Brown, E. J. Penn, K. Thomas, G. Kulnis, B. Hallis, M. Carroll, S. Funnell, S. Charlton, *Nat. Protoc.* **2021**, *16*, 3114.
[3] M. Pieri, M. Infantino, M. Manfredi, M. Nuccetelli, V. Grossi, B. Lari, F. Tomassetti, S. Sarubbi, E. Russo, A. Amedei, M. Benucci, P. Casprini, L. Stacchini, C. Castilletti, S. Bernardini, *Front. Biosci. Landmark* **2022**, *27*(2), 074.
[4] C. Chen, J. Liang, H. Hu, X. Li, L. Wang, Z. Wang, *Anal. Biochem.* **2023**, *673*, 115199.
[5] B. J. Cohen, D. Doblas, N. Andrews, *Vaccine* **2008**, *26*(50), 6392.
[6] J. R. Izac, E. J. Kwee, L. Tian, E. Elsheikh, A. K. Gaigalas, J. T. Elliott, L. Wang, *Int. J. Mol. Sci.* **2023**, *24*(15), 12332.
[7] R. Kalkeri, Z. Cai, S. Lin, J. Farmer, Y. V. Kuzmichev, F. Koide, *Microorganisms* **2021**, *9*(8), 1744.
[8] J. Bi, H. Wang, H. Pei, Q. Han, N. Feng, Q. Wang, X. Wang, Z. Wang, S. Wei, L. Ge, M. Wu, H. Liang, S. Yang, F. Yan, Y. Zhao, X. Xia, *Front. Microbiol.* **2022**, *13*, 927122.
[9] J. Nie, Q. Li, J. Wu, C. Zhao, H. Hao, H. Liu, L. Zhang, L. Nie, H. Qin, M. Wang, Q. Lu, X. Li, Q. Sun, J. Liu, C. Fan, W. Huang, M. Xu, Y. Wang, *Nat. Protoc.* **2020**, *15*, 3699.
[10] X. Sun, S. L. Roth, M. A. Bialecki, G. R. Whittaker, *Future Virol.* **2010**, *5*(1), 85.
[11] S. Rehman, S. Bishnoi, R. Roy, A. Kumari, H. Jayakumar, S. Gupta, P. Kar, A. K. Pattnaik, D. Nayak, *ACS Omega* **2022**, *7*(27), 32840.
[12] S. Balachandran, M. Porosnicu, G. N. Barber, *J. Virol.* **2001**, *75*, 3474.
[13] S. A. Kopecky, D. S. Lyles, *J. Virol.* **2003**, *77*, 4658.
[14] M. Hoffmann, Y.-J. Wu, M. Gerber, M. Berger-Rentsch, B. Heimrich, M. Schwemmle, G. Zimmer, *J. Gen. Virol.* **2010**, *91*, 2782.
[15] X. Wang, C. H. Chen, S. Badeti, J. H. Cho, A. Naghizadeh, Z. Wang, D. Liu, *Cell Biosci.* **2021**, *11*, 114.
[16] J. M. Condor Capcha, G. Lambert, D. M. Dykxhoorn, A. G. Salerno, J. M. Hare, M. A. Whitt, S. Pahwa, D. T. Jayaweera, L. A. Shehadeh, *Front. Cardiovasc. Med.* **2021**, *7*, 618651.
[17] M. Hoffmann, H. Kleine-Weber, S. Schroeder, N. Krüger, T. Herrler, S. Erichsen, T. S. Schiergens, G. Herrler, N. H. Wu, A. Nitsche, M. A. Müller, C. Drosten, S. Pöhlmann, *Cell* **2020**, *181*(2), 271.
[18] M. Berger Rentsch, G. Zimmer, *PLoS One* **2011**, *6*(10), e25858.
[19] U. Hofmann, S. Michaelis, T. Winckler, J. Wegener, K.-H. Feller, *Biosens. Bioelectron.* **2013**, *39*(1), 156.
[20] I. Giaever, C. R. Keese, *Proc. Natl Acad. Sci.* **1984**, *81*(12), 3761.
[21] L. Riepler, A. Rössler, A. Falch, A. Volland, W. Borena, D. von Laer, J. Kimpel, *Vaccines* **2020**, *9*(1), 13.
[22] M. A. Whitt, *J. Virol. Methods* **2010**, *169*(2), 365.
[23] S. Einhauser, D. Peterhoff, S. Beileke, F. Günther, H.-H. Niller, P. Steininger, A. Knöll, K. Korn, M. Berr, A. Schütz, S. Wiegrebe, K. J. Stark, A. Gessner, R. Burkhardt, M. Kabesch, H. Schedl, H. Küchenhoff, A. B. Pfahlberg, I. M. Heid, O. Gefeller, K. Überla, R. Wagner, *Viruses* **2022**, *14*, 1168.
[24] R. Wagner, D. Peterhoff, S. Beileke, F. Günther, M. Berr, S. Einhauser, A. Schütz, H. H. Niller, P. Steininger, A. Knöll, M. Tenbusch, C. Maier, K. Korn, K. J. Stark, A. Gessner, R. Burkhardt, M. Kabesch, H. Schedl, H. Küchenhoff, A. B. Pfahlberg, I. M. Heid, O. Gefeller, K. Überla, *Viruses* **2021**, *13*, 1118.
[25] J. Wegener, C. R. Keese, I. Giaever, *Exp. Cell Res.* **2000**, *259*(1), 158.
[26] https://www.biophysics.com/cultureware.php#96W1E (accessed February 17, 2024).
[27] C. R. Keese, J. Wegener, S. R. Walker, I. Giaever, *Proc. Natl Acad. Sci.* **2004**, *101*(6), 1554.
[28] P. Gadaleta, M. Vacotto, F. Coulombié, *Virus Res.* **2002**, *86*(1–2), 87.
[29] S. Arndt, J. Seebach, K. Psathaki, H. J. Galla, J. Wegener, *Biosens. Bioelectron.* **2004**, *19*(6), 583.

[30] A. M. Munis, M. Tijani, M. Hassall, G. Mattiuzzo, M. K. Collins, Y. Takeuchi, *J. Virol.* **2018**, *92*(23), e00900-18.
[31] H. Gubler *Methods for statistical analysis, quality assurance and management of primary high-throughput screening data* (Eds: G. Folkers, J. Hüser, R. Mannhold, H Kubinyi), Wiley-VCH, **2006**, p. 151.
[32] M. Lay Mendoza, M. Acciani, C. Levit, C. Santa Maria, M. Brindley, *Viruses* **2020**, *12*(12), 1457.
[33] V. Blay, B. Tolani, S. P. Ho, M. R. Arkin, *Drug Discov. Today* **2020**, *25*(10), 1807.
[34] I. Giaever, C. R. Keese, *Proc. Natl Acad. Sci.* **1991**, *88*, 7896.
[35] I. Voiculescu, F. Li, A. N. Nordin, *IEEE Sens. J.* **2021**, *21*(5), 5612.

SUPPORTING INFORMATION

Additional supporting information can be found online in the Supporting Information section at the end of this article.

How to cite this article: A. -. K. Mildner, S. Einhauser, S. Michaelis, K. R. v. Bieberstein, R. Wagner, J. Wegener, *Appl. Res.* **2024**, e2400097.
https://doi.org/10.1002/appl.202400097